Journal of Catalysis 277 (2011) 36–45

Contents lists available at ScienceDirect

Journal of Catalysis

journal homepage: www.elsevier.com/locate/jcat

Catalytic hydrogenation of alkenes on acidic zeolites: Mechanistic connections to monomolecular alkane dehydrogenation reactions

Rajamani Gounder, Enrique Iglesia *

Department of Chemical Engineering, University of California at Berkeley, Berkeley, CA 94720, United States

ARTICLE INFO

Article history:
Received 31 August 2010
Revised 4 October 2010
Accepted 13 October 2010
Available online 17 November 2010

Keywords:
Alkene hydrogenation
Alkane dehydrogenation
Brønsted acid catalysis
De Donder relations
Microscopic reversibility
Monomolecular alkane activation
Zeolite catalysis

ABSTRACT

Brønsted acid sites in zeolites (H-FER, H-MFI, H-MOR) selectively hydrogenate alkenes in excess H_2 at high temperatures (>700 K) and at rates proportional to alkene and H_2 pressures. This kinetic behavior and the De Donder equations for non-equilibrium thermodynamics show that, even away from equilibrium, alkene hydrogenation and monomolecular alkane dehydrogenation occur on predominantly uncovered surfaces via microscopically reverse elementary steps, which involve kinetically-relevant $(C–H–H)^+$ carbonium-ion-like transition states in both directions. As a result, rate constants, activation energies and activation entropies for these two reactions are related by the thermodynamics of the overall stoichiometric gas-phase reaction. The ratios of rate constants for hydrogenation and dehydrogenation reactions do not depend on the identity or reactivity of active sites; thus, sites within different zeolite structures (or at different locations within a given zeolite) that favor alkane dehydrogenation reactions, because of their ability to stabilize the required transition states, also favor alkene hydrogenation reactions to the exact same extent. These concepts and conclusions also apply to monomolecular alkane cracking and bimolecular alkane–alkene reaction paths on Brønsted acids and, more generally, to any forward and reverse reactions that proceed via the same kinetically-relevant step on vacant surfaces in the two directions, even away from equilibrium. The evidence shown here for the sole involvement of Brønsted acids in the hydrogenation of alkoxides with H_2 is unprecedented in its mechanistic clarity and thermodynamic rigor. The scavenging of alkoxides via direct H-transfer from H_2 indicates that H_2 can be used to control the growth of chains and the formation of unreactive deposits in alkylation, oligomerization, cracking and other acid-catalyzed reactions.

Published by Elsevier Inc.

1. Introduction

The catalytic cracking and dehydrogenation of alkanes on Brønsted acid sites within zeolites have been shown by experiment [1–5] and theory [6–9] to occur via monomolecular routes at high temperatures (>623 K) and low conversions (<2%) [10]. These paths involve protonation at C–C or C–H bonds in alkanes, respectively, to form $(C–C–H)^+$ or $(C–H–H)^+$ carbonium-ion-like transition states in their respective kinetically-relevant bond scission steps [2]. Cracking and dehydrogenation of alkanes (C_3H_8, n-C_4H_{10}, i-C_4H_{10}) via monomolecular routes at these conditions occur exclusively on Brønsted acid sites in H-FER, H-MFI and H-MOR, consistent with rates proportional to the proton density in these materials but not with the number of metal or Lewis acid impurity sites [2,3]. On all zeolites, the differences between cracking and dehydrogenation activation energies of a given alkane equal the difference in gas-phase proton affinities of its C–C and C–H bonds, as expected from thermochemical cycle analyses of transition state ion-pairs for cracking and dehydrogenation paths catalyzed by Brønsted acids (Section S.1, Supporting information) [2,3].

The hydrogenation of alkenes by H_2 on acidic zeolites, however, is typically attributed to metals [11–16] or cations [17,18] introduced deliberately or present as adventitious impurities [19,20]. Yet, the reactivity of Brønsted acid sites in monomolecular alkane dehydrogenation would make such sites plausible candidates as catalysts for alkene hydrogenation with H_2 via carbonium-ion-like transition states, as proposed, but not shown unequivocally, on liquid superacids [21–23] and solid acids [18,24,25]. This expectation would be justified rigorously for any general chemical reaction only *at equilibrium*, conditions at which reactions occur via identical mechanistic sequences in forward and reverse directions, as dictated by the principle of microscopic reversibility [26,27]. Such requirements hold even *away from equilibrium* for elementary steps, because they involve a single energy barrier that must be surmounted in both directions along the reaction coordinate.

We provide evidence here that Brønsted acid sites in zeolites catalyze alkene hydrogenation with H_2, even at conditions far away from equilibrium, via the microscopic reverse of monomolecular

* Corresponding author. Fax: +1 510 642 4778.
E-mail address: iglesia@berkeley.edu (E. Iglesia).

0021-9517/$ - see front matter Published by Elsevier Inc.
doi:10.1016/j.jcat.2010.10.013

alkane dehydrogenation paths and at rates constrained by the thermodynamics of the stoichiometric gas-phase reaction. Rate constants, activation energies and activation entropies for propene hydrogenation and monomolecular propane dehydrogenation are interpreted rigorously using common elementary steps and De Donder relations that describe the rates of elementary steps as a function of their chemical affinity, the relevant metric for their distance from equilibrium. We use these mechanistic insights to show that intrazeolite locations and channel structures that lead to more active Brønsted acid sites do so to the same extent for monomolecular propane dehydrogenation and propene hydrogenation reactions, regardless of their respective distances from equilibrium. These conclusions would seem at first glance to extend the principle of microscopic reversibility beyond its intended description of chemical reactions at equilibrium, but represent, in fact, a not altogether uncommon example of chemical reactions that involve a single kinetically-relevant elementary step on predominantly vacant surfaces, for which such principles apply at all distances from equilibrium.

2. Methods

2.1. Catalyst synthesis and characterization

NH_4^+-zeolites were treated in flowing dry air (2.5 $cm^3\ g^{-1}\ s^{-1}$, zero grade, Praxair) by heating to 773 K (0.0167 K s^{-1}) and holding for 4 h to prepare H-zeolites, which were then pelleted, crushed and sieved to retain 180–250 μm (60–80 mesh) aggregates. The zeolite samples used are described in Table 1 together with the relevant characterization data. The notation describes their fractional H^+ and Na^+ content at exchange sites, their framework structure and their provenance. Methods to prepare Na^+-exchanged zeolites, measure elemental composition, and collect ^{27}Al NMR and infrared spectra have been reported elsewhere [2]. The number of Brønsted acid sites in Na^+-exchanged samples was determined by the difference in the number of framework Al atoms and exchanged Na^+ cations.

2.2. Catalytic rate measurements

Procedures for measuring monomolecular alkane dehydrogenation rates have been reported elsewhere [2]. Alkene hydrogenation rates were measured in a plug-flow tubular quartz reactor under differential conditions (<5% conversion). Before rate measurements, catalysts (0.01–0.10 g) were treated at 803 K (0.0167 K s^{-1}) in a 5% O_2/95% He mixture (16.7 $cm^3\ g^{-1}\ s^{-1}$, 99.999%, Praxair) for 2 h and then in pure He flow (16.7 $cm^3\ g^{-1}\ s^{-1}$, 99.999%, Praxair) for 0.5 h while propene (1% C_3H_6, 5% Ar, 94% He, Praxair, 99.5% purity) and H_2 (99.999%, Praxair) reactants were transferred to a gas chromatograph (Agilent HP-6890GC) via heated lines (423 K) for calibration purposes. Reactants and products were separated using GS-AL/KCl capillary (0.530 mm ID × 50 m; Agilent) and HayeSep DB packed (100–120 mesh, 10 ft.; Sigma–Aldrich) columns and detected using flame ionization and thermal conductivity detection, respectively. Reactants were diluted with He (99.999%, Praxair) to vary the pressures and molar rates of C_3H_6 (0.01–0.05 kPa; 10^{-7}–10^{-6} (mol C_3H_6) $g^{-1}\ s^{-1}$) and H_2 (10–120 kPa; 10^{-4}–10^{-3} (mol H_2) $g^{-1}\ s^{-1}$) and to maintain high H_2/C_3H_6 feed molar ratios (>1000). Rate constants measured between 718 K and 778 K were used to estimate activation energies and pre-exponential factors. On all catalysts, steady-state rates and selectivities measured after ~12 h on stream were similar (within 5%) to their initial values, indicating that kinetic data were unaffected by deactivation.

3. Results and discussion

3.1. Monomolecular alkane dehydrogenation on acidic zeolites

Monomolecular alkane dehydrogenation proceeds via quasi-equilibrated adsorption of alkanes within zeolite voids that contain Brønsted acid sites (Step 1, Scheme 1), the subsequent formation of $(C\text{–}H\text{–}H)^+$ carbonium-ion-like transition states in kinetically-relevant C–H scission steps (Step 2, Scheme 1), and quasi-equilibrated desorption of alkene and H_2 products (Steps 3–5, Scheme 1) [2]. The temperatures and pressures required for monomolecular alkane activation lead to unoccupied H^+ sites as the most abundant surface intermediate (MASI) [2] and to low intrazeolite alkane concentrations that are proportional to gas-phase pressures.

Propane dehydrogenation rates (per H^+; 718–778 K; <2% conversion) on acidic zeolites (H-FER, H-MFI, H-MOR) are proportional to C_3H_8 pressures (Fig. 1), consistent with an equation for monomolecular propane dehydrogenation rates (per H^+) derived from the mechanistic assumptions described earlier:

$$\vec{r}_D = K_1 k_2 P_{C_3H_8} = k_{meas,D} P_{C_3H_8}. \quad (1)$$

In this equation, $k_{meas,D}$ is the effective first-order dehydrogenation rate constant, K_1 is the equilibrium constant relating intrazeolite C_3H_8 concentrations to extrazeolite C_3H_8 pressures, and k_2 is the rate constant for the step that forms $C_3H_7^+$ and H_2 species within zeolites via $(C_3H_9)^+$ carbonium-ion-like transition states. Dehydrogenation rate constants ($k_{meas,D}$) can be expressed in terms of measured activation energies ($E_{meas,D}$) and pre-exponential factors ($A_{meas,D}$):

$$k_{meas,D} = A_{meas,D} \exp(-E_{meas,D}/RT). \quad (2)$$

Temperature effects on $k_{meas,D}$ include contributions from K_1 and k_2, and $E_{meas,D}$ reflects enthalpy differences between $(C_3H_9)^+$ carbonium-ion-like transition states (Step 2, Scheme 1) within zeolite channels and C_3H_8 reactants in the extrazeolite fluid phase (as depicted in Scheme 2):

Table 1
Characterization of zeolite samples used in this study.

Zeolite	Source	Si/Al ratio[a]	Na/Al ratio[a]	Al_{EF}[b] (%)	$X_{8\text{-MR}}$[c]	$X_{12\text{-MR}}$[c]
$H_{100}Na_0$-FER-Z	Zeolyst	10.3	0.002	15	–	–
$H_{100}Na_0$-MFI-Z	Zeolyst	16.5	0.004	12	–	–
$H_{100}Na_0$-MOR-T	Tosoh	8.9	0.001	19	0.78	0.22
$H_{100}Na_0$-MOR-S	Sud-Chemie	10.1	0.001	21	0.60	0.40
$H_{100}Na_0$-MOR-Z	Zeolyst	10.0	0.001	22	0.56	0.44
$H_{83}Na_{17}$-MOR-Z	Zeolyst	10.0	0.17	22	0.36	0.64
$H_{73}Na_{27}$-MOR-Z	Zeolyst	10.0	0.27	22	0.27	0.73
$H_{59}Na_{41}$-MOR-Z	Zeolyst	10.0	0.41	22	0.20	0.80
$H_{38}Na_{62}$-MOR-Z	Zeolyst	10.0	0.62	22	0.17	0.83

[a] Determined from elemental analysis (ICP-OES; Galbraith Laboratories).
[b] Extra-framework Al content (Al_{EF}) determined from ^{27}Al MAS NMR spectra; details in [2].
[c] Fraction of H^+ sites in 8-MR or 12-MR locations on MOR samples determined from infrared spectral band deconvolution (Section S.3, Supporting information).

$$RH_2\,(g) \rightleftharpoons R\,(g) + H_2\,(g)$$

			σ
1.	$RH_2\,(g)$	$\underset{k_{-1}}{\overset{k_1}{\rightleftharpoons}}$ $RH_2\,(z)$	1
2.	$RH_2\,(z) + H^+Z^-$	$\underset{k_{-2}}{\overset{k_2}{\rightleftharpoons}}$ $RH^+Z^- + H_2\,(z)$	1
3.	RH^+Z^-	$\underset{k_{-3}}{\overset{k_3}{\rightleftharpoons}}$ $R\,(z) + H^+Z^-$	1
4.	$R\,(z)$	$\underset{k_{-4}}{\overset{k_4}{\rightleftharpoons}}$ $R\,(g)$	1
5.	$H_2\,(z)$	$\underset{k_{-5}}{\overset{k_5}{\rightleftharpoons}}$ $H_2\,(g)$	1

Scheme 1. Catalytic cycle for monomolecular alkane (RH_2) dehydrogenation and for alkene (R) hydrogenation with H_2 on acidic zeolites involving gas-phase species (g), adsorbates at framework Al sites (Z^-), and species adsorbed within zeolite channels near framework Al sites (z). Stoichiometric numbers (σ) shown for each elementary step.

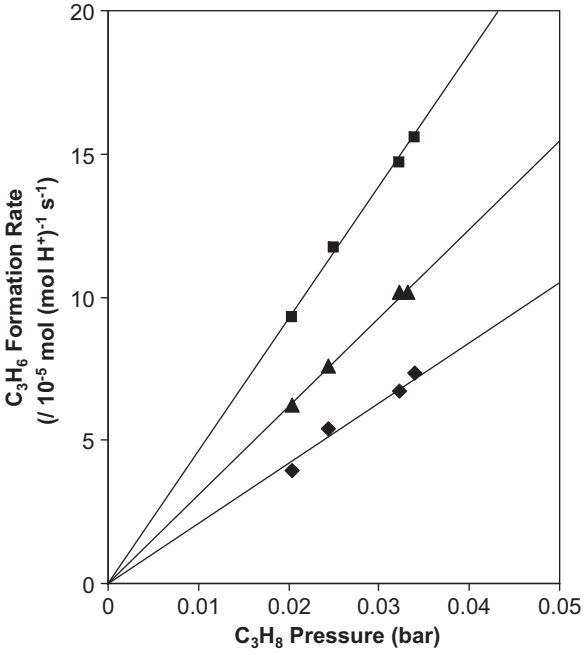

Fig. 1. Dependence of propene formation rates (748 K) on propane pressure on $H_{100}Na_0$-FER-Z (▲), $H_{100}Na_0$-MFI-Z (■), and $H_{100}Na_0$-MOR-Z (♦) during monomolecular propane dehydrogenation reactions.

$$E_{meas,D} = \Delta H_1 + E_2 = \Delta H^{\circ}_{\ddagger,2} - \Delta H^{\circ}_{H^+Z^-} - \Delta H^{\circ}_{C_3H_8(g)}. \quad (3)$$

$A_{meas,D}$ also includes contributions from K_1 and k_2 and reflects entropy differences between the transition state for Step 2 and gaseous C_3H_8 reactants. This measured activation entropy ($\Delta S_{meas,D}$), corrected for the number of C–H bonds in the reactant alkane (n_B) [2], is given by:

$$\Delta S_{meas,D} = R\left[\ln\left(A_{meas,D}/n_B\right) - \ln\left(k_B T/h\right)\right] = \Delta S^{\circ}_{\ddagger,2} - \Delta S^{\circ}_{H^+Z^-} - \Delta S^{\circ}_{C_3H_8(g)}. \quad (4)$$

The measured rate parameters for monomolecular propane dehydrogenation are reported on each sample as $k_{meas,D}$, $E_{meas,D}$ and $\Delta S_{meas,D}$ in Tables 2 and 3.

3.2. Catalytic hydrogenation of alkenes on acidic zeolites

Reactions of propene with excess H_2 ($H_2/C_3H_6 > 2500$) at temperatures also used for monomolecular propane dehydrogenation (718–778 K) formed propane with high selectivity (>80%; Fig. 2) on H-FER, H-MFI and H-MOR, irrespective of zeolite provenance or Na^+ content. Propane formation rates (per H^+) increased linearly with C_3H_6 and H_2 pressures (Fig. 3), consistent with rates expected for low intrazeolite H_2 and C_3H_6 concentrations in equilibrium with their extrazeolite pressures and for kinetically-relevant reactions of C_3 intermediates, either as bound alkoxides, carbenium ions or physisorbed alkenes, with intrazeolite H_2 species (Step 2, Scheme 1):

$$\overleftarrow{r}_H = k_{-2}K_3^{-1}K_4^{-1}K_5^{-1}P_{C_3H_6}P_{H_2} = k_{meas,H}P_{C_3H_6}P_{H_2}. \quad (5)$$

Here, $k_{meas,H}$ is the effective second-order hydrogenation rate constant, K_3, K_4, and K_5 are equilibrium constants relating intrazeolite concentrations of $C_3H_7^+$, C_3H_6 and H_2 species to C_3H_6 and H_2 gas-phase pressures, and k_{-2} is the rate constant for the formation of intrazeolitic C_3H_8 species via $(C_3H_9)^+$ carbonium-ion-like transition states. We note that the identity of the C_3 intermediate involved in the kinetically-relevant step (Step 2, Scheme 1) cannot be determined from kinetic data, which only indicate that C_3 species present as alkoxides, carbenium ions or physisorbed alkenes are in quasi-equilibrium with gaseous C_3H_6; we refer to the intermediate involved in Step 2 (Scheme 1) as an alkoxide to facilitate the discussion that follows.

Rates of propane formation were influenced only weakly by space velocity and gave large values after extrapolation to zero residence time (Fig. 4), consistent with its formation via direct hydrogenation of propene. Methane and ethylene were formed in nearly equimolar ratios also as primary products (Fig. 4), but with much lower selectivities that decreased with increasing H_2 pressure ($H_2/C_3H_6 > 2000$; Fig. 2). These minority products may form either via monomolecular cracking of propoxide species [28–30] to form C_2H_4 and CH_3^+ surface species that subsequently react with H_2 to form CH_4, or via interconversion of $(C–H–H)^+$ dehydrogenation–hydrogenation transition states to the $(C–C–H)^+$ transition states involved in monomolecular cracking to form C_2H_4 and CH_4. At lower H_2 pressures ($H_2/C_3H_6 < 2000$), C_{4+} molecules become detectable and C_2H_4/CH_4 ratios become larger than unity, apparently via β-scission of larger chains formed by C_3H_6 oligomerization with propoxides or with methyl groups stranded by β-scission reactions of propoxides to form C_2H_4 in stoichiometric excess ($C_2H_4/CH_4 > 1$).

Temperature effects on $k_{meas,H}$ reflect enthalpy differences between hydrogenation transition states (Step 2, Scheme 1) and alkene and H_2 reactants in the external fluid phase:

$$E_{meas,H} = E_{-2} - \Delta H_3 - \Delta H_4 - \Delta H_5 = \Delta H^{\circ}_{\ddagger,-2} - \Delta H^{\circ}_{H^+Z^-} - \Delta H^{\circ}_{C_3H_6(g)} - \Delta H^{\circ}_{H_2(g)}, \quad (6)$$

as also shown in Scheme 2 when the same transition state is involved in propane dehydrogenation and propene hydrogenation, because the kinetically-relevant step is the same (albeit in reverse directions) for these two reactions. The same approach leads to expressions for measured activation entropies for hydrogenation ($\Delta S_{meas,H}$), which reflect entropy differences between the hydrogenation transition state (Step 2, Scheme 1) and extrazeolite C_3H_6 and H_2 reactants:

$$\Delta S_{meas,H} = R\left[\ln\left(A_{meas,H}/n_B\right) - \ln(k_B T/h)\right] = \Delta S^{\circ}_{\ddagger,-2} - \Delta S^{\circ}_{H^+Z^-} - \Delta S^{\circ}_{C_3H_6(g)} - \Delta S^{\circ}_{H_2(g)}. \quad (7)$$

These rate parameters ($k_{meas,H}$, $E_{meas,H}$, $\Delta S_{meas,H}$) for propene hydrogenation on each zeolite catalyst are also shown in Tables 2 and 3.

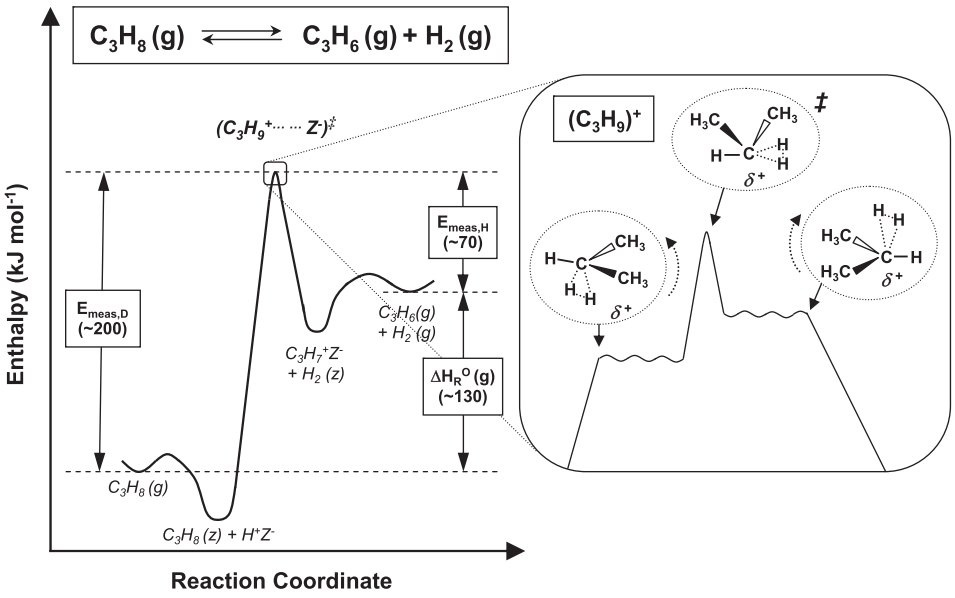

Scheme 2. Relative enthalpies along the reaction coordinate of molecules in the gas and intrazeolite phases, and of $(C_3H_9)^+$ carbonium-ion-pairs stabilized within zeolite channels. Enthalpy differences are reflected in measured activation barriers for monomolecular propane dehydrogenation ($E_{meas,D}$) and for propene hydrogenation ($E_{meas,H}$), and in the gas-phase reaction enthalpy $\left(\Delta H_R^o(g)\right)$ (approximate values in parentheses). Plausible carbonium-ion structures involved in the reaction coordinate are also depicted.

Table 2
Rate constants for monomolecular propane dehydrogenation ($k_{meas,D}$; mol (mol $H^+)^{-1}$ s^{-1} (bar $C_3H_8)^{-1}$) and for propene hydrogenation ($k_{meas,H}$; mol (mol $H^+)^{-1}$ s^{-1} (bar $C_3H_6)^{-1}$ (bar $H_2)^{-1}$) and their ratio ($k_{meas,D}/k_{meas,H}$; bar) on acidic zeolites at 748 K. Mean value of $k_{meas,D}/k_{meas,H}$ on all samples is 0.017 ± 0.001 bar (95% confidence interval).

Zeolite	$k_{meas,D}$	$k_{meas,H}$	$k_{meas,D}/k_{meas,H}$
$H_{100}Na_0$-FER-Z	0.0031	0.22	0.014
$H_{100}Na_0$-MFI-Z	0.0046	0.26	0.018
$H_{100}Na_0$-MOR-T	0.0029	0.17	0.018
$H_{100}Na_0$-MOR-S	0.0018	0.10	0.018
$H_{100}Na_0$-MOR-Z	0.0021	0.12	0.018
$H_{83}Na_{17}$-MOR-Z	0.0012	0.075	0.016
$H_{73}Na_{27}$-MOR-Z	0.00085	0.044	0.019
$H_{59}Na_{41}$-MOR-Z	0.00065	0.041	0.016
$H_{38}Na_{62}$-MOR-Z	0.00058	0.035	0.017

Monomolecular propane dehydrogenation (Eq. (1)) and propene hydrogenation (Eq. (5)) rate equations reflect the law of mass action for the stoichiometric reaction in their respective directions (Scheme 1). Thus, the ratio of hydrogenation and dehydrogenation rates depends on the same combined pressure terms as in the equilibrium expression for the overall chemical reaction ($(C_3H_6)(H_2)/(C_3H_8)$; Section S.2, Supporting information). This algebraic resemblance, by itself, is insufficient to establish a mechanistic connection between their respective sequences of elementary steps (i.e., Scheme 1) or to relate the measured rate constants ($k_{meas,D}$, $k_{meas,H}$) to specific steps as they appear in Eqs. (1) and (5), or to the equilibrium constant for the overall reaction, because these rate constants are measured at different conditions and far from equilibrium in their respective directions. In what follows, we provide evidence that alkane dehydrogenation and alkene hydrogenation paths do, in fact, proceed via the same sequence of elementary steps (Scheme 1) by interpreting rate constants in mechanistic terms and using the De Donder relations to connect kinetic parameters (k_{meas}, E_{meas}, ΔS_{meas}) for these two reactions.

3.3. The De Donder formalism for rates of elementary steps and their sequences

The net rate of an elementary step (r_i) reflects the difference between its forward ($\vec{r_i}$) and reverse ($\overleftarrow{r_i}$) rates:

Table 3
Measured activation energies (E_{meas}; kJ mol^{-1}) and entropies (ΔS_{meas}; J mol^{-1} K^{-1}) for propane dehydrogenation and for propene hydrogenation on acidic zeolites; uncertainties correspond to a 95% confidence interval. Mean values of ($E_{meas,D} - E_{meas,H}$) and ($\Delta S_{meas,D} - \Delta S_{meas,H}$) on all samples are 127 ± 8 kJ mol^{-1} and 134 ± 11 J mol^{-1} K^{-1}, respectively (95% confidence interval).

Zeolite	$E_{meas,D}$[a]	$E_{meas,H}$[b]	$E_{meas,D} - E_{meas,H}$	$\Delta S_{meas,D}$[c]	$\Delta S_{meas,H}$[d]	$\Delta S_{meas,D} - \Delta S_{meas,H}$
$H_{100}Na_0$-FER-Z	195	76	119	−57	−180	123
$H_{100}Na_0$-MFI-Z	204	90	114	−42	−160	118
$H_{100}Na_0$-MOR-T	189	58	131	−66	−206	140
$H_{100}Na_0$-MOR-S	192	56	136	−66	−213	147
$H_{100}Na_0$-MOR-Z	198	77	121	−56	−184	128
$H_{83}Na_{17}$-MOR-Z	201	71	130	−57	−195	138
$H_{73}Na_{27}$-MOR-Z	201	75	126	−60	−194	134
$H_{59}Na_{41}$-MOR-Z	196	60	136	−69	−215	146

[a] ±7 kJ mol^{-1}.
[b] ±9 kJ mol^{-1}.
[c] ±10 J mol^{-1} K^{-1}.
[d] ±11 J mol^{-1} K^{-1}.

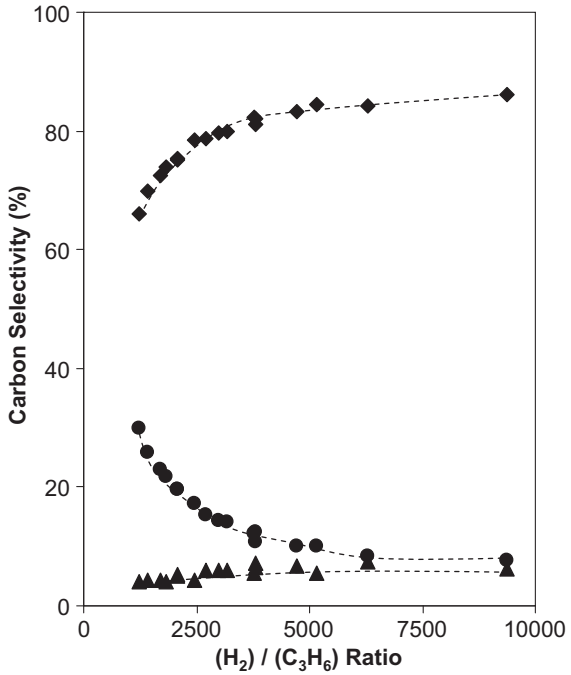

Fig. 2. Carbon selectivity to C_3H_8 (♦), C_2H_4 (●), and CH_4 (▲) products formed during propene hydrogenation with varying H_2/C_3H_6 feed ratio at 748 K on $H_{100}Na_0$-MOR-Z.

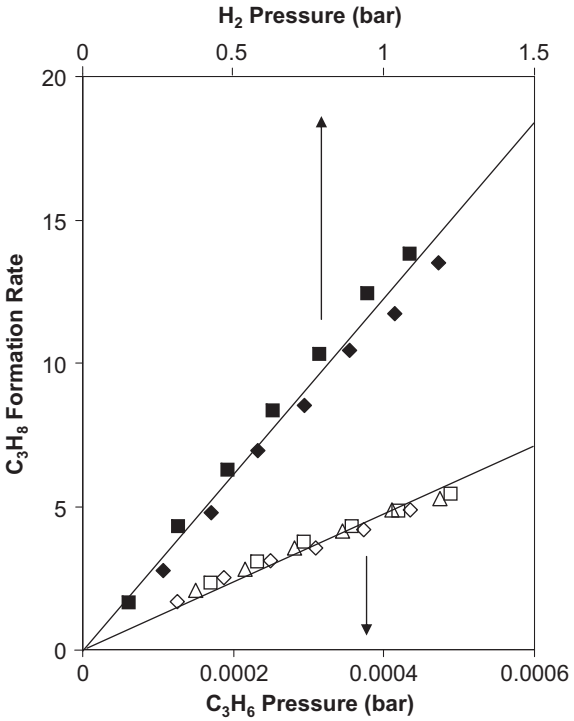

Fig. 3. Dependence of C_3H_8 formation rates (748 K) on C_3H_6 pressure ($\times 10^5$ mol (mol H^+)$^{-1}$ s^{-1} (bar H_2)$^{-1}$; ◇: $P(H_2)$ = 1.2 bar; □: $P(H_2)$ = 0.9 bar; △: $P(H_2)$ = 0.6 bar) and H_2 pressure ($\times 10^2$ mol (mol H^+)$^{-1}$ s^{-1} (bar C_3H_6)$^{-1}$; ♦: $P(C_3H_6)$ = 0.0003 bar; ■: $P(C_3H_6)$ = 0.0001 bar) on $H_{100}Na_0$-MOR-Z.

$$r_i = \vec{r}_i - \overleftarrow{r}_i . \tag{8}$$

The De Donder equation [31,32] relates forward and reverse rates to chemical affinities (A_i) for a given step, which are defined as $(-\partial G/\partial \xi)_{T,P}$ with G denoting the Gibbs free energy and ξ the extent of reaction:

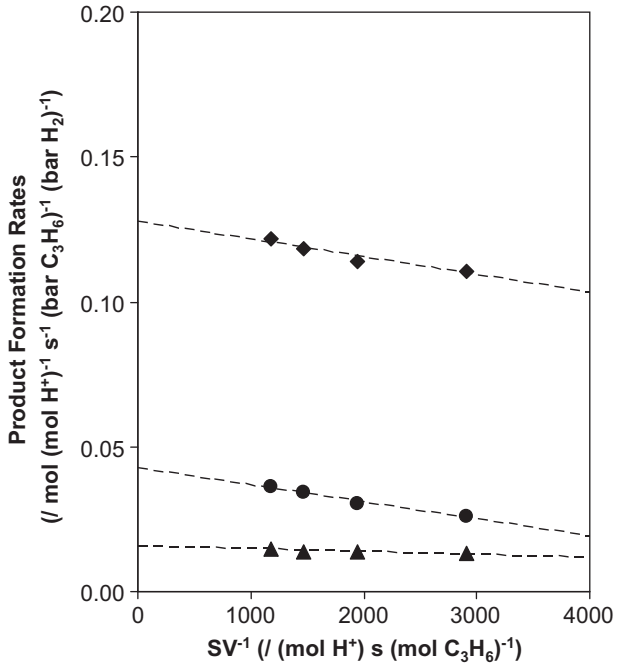

Fig. 4. Rates of formation of C_3H_8 (♦), C_2H_4 (●), and CH_4 (▲) at different C_3H_6 space velocities (SV) (3–6% C_3H_6 conversion) on $H_{100}Na_0$-MOR-Z at 748 K and a 4000/1 H_2/C_3H_6 feed ratio.

$$\vec{r}_i / \overleftarrow{r}_i = \exp(A_i/RT). \tag{9}$$

Elementary step reaction rates must also obey the law of mass action because they occur as written, and the chemical affinity is given by:

$$A_i = RT \ln\left(K_i \prod_j a_j^{-\nu_j}\right), \tag{10}$$

where a_j and ν_j are the thermodynamic activity and molecularity of the species j involved in step i, and where ν_j is positive for products and negative for reactants. K_i is the equilibrium constant for the step, which is given, in turn, by the ratio of its forward (k_i) and reverse (k_i) rate constants:

$$K_i = \frac{\vec{k}_i}{\overleftarrow{k}_i}. \tag{11}$$

The De Donder equation (Eq. (9)) accounts rigorously for the consequences of thermodynamic equilibrium and of reactant and product thermodynamic activities on the net rate of any elementary step in a catalytic sequence [33–36]; the sign of A_i prescribes the direction in which the chemical transformation indicated by that step will occur. The net rate of each elementary step is then given by Eqs. (8)–(10) in terms of the approach to equilibrium parameter for the ith step (η_i) as:

$$r_i = \vec{r}_i \left(1 - \frac{1}{K_i \prod_j a_j^{-\nu_j}}\right) = \vec{r}_i (1 - \eta_i). \tag{12}$$

The value of η_i approaches zero far away from equilibrium and unity as a step reaches equilibrium.

Catalytic reactions occur, however, via a sequence of elementary steps that form reactive intermediates on active sites, transform them chemically, and ultimately desorb them as products to regenerate sites for subsequent turnovers. The pseudo-steady-state hypothesis (PSSH) for all adsorbed species requires that the

net rate of each elementary step be related to that of the overall reaction (r) by:

$$\vec{r}_i - \overleftarrow{r}_i = \sigma_i(\vec{r}_i - \overleftarrow{r}) = \sigma_i r, \tag{13}$$

in which σ_i is the stoichiometric number for Step i, defined as the number of times it must occur to complete one catalytic turnover. Applying Eq. (9) to each elementary step in a catalytic sequence allows the De Donder formalism to be extended from elementary steps to single path catalytic sequences [36]:

$$\frac{\vec{r}}{\overleftarrow{r}} = \frac{\prod \vec{r}_i}{\prod \overleftarrow{r}_i} = \exp\left(\sum A_i \Big/ RT\right) = \exp(A/\bar{\sigma}RT), \tag{14}$$

where A represents the chemical affinity for the overall reaction sequence:

$$A = \sum_i \sigma_i A_i, \tag{15}$$

and $\bar{\sigma}$ is an affinity-averaged stoichiometric number for the catalytic sequence:

$$\bar{\sigma} = \sum_i \sigma_i A_i \Big/ \sum_i A_i. \tag{16}$$

The fact that elementary steps are reversible (Eq. (9)) implies that a single path catalytic sequence must also occur in both forward and reverse directions at the respective rates given by Eq. (14), *at a given set of reaction conditions* (T, P_j). Moreover, forward ($\vec{k}$) and reverse ($\overleftarrow{k}$) rate constants must be related to the equilibrium constant (K_R) for the overall reaction [36] by:

$$\vec{k} \,/\, \overleftarrow{k} = K_R^{1/\bar{\sigma}}. \tag{17}$$

When all kinetically-relevant steps in a catalytic sequence have stoichiometric numbers of unity, as is the case for hydrogenation–dehydrogenation reactions (Scheme 1), Eqs. (14) and (17) become indistinguishable from those derived for a single elementary step, irrespective of the concentrations of reactants and products relative to their equilibrium values.

3.4. Mechanistic connections between alkane dehydrogenation and alkene hydrogenation

The application of Eq. (14) to the alkane dehydrogenation sequence in Scheme 1 and with forward and reverse rates for elementary steps given by the law of mass action results in:

$$\frac{\vec{r}_D}{\overleftarrow{r}_H} = \frac{\vec{r}_1}{\overleftarrow{r}_1}\frac{\vec{r}_2}{\overleftarrow{r}_2}\frac{\vec{r}_3}{\overleftarrow{r}_3}\frac{\vec{r}_4}{\overleftarrow{r}_4}\frac{\vec{r}_5}{\overleftarrow{r}_5} = \frac{k_1 a_{RH_2(g)} k_2 a_{RH_2(z)} a_{H^+Z^-} k_3 a_{RH^+Z^-} k_4 a_{R(z)} k_5 a_{H_2(z)}}{k_{-1} a_{RH_2(z)} k_{-2} a_{RH^+Z^-} a_{H_2(z)} k_{-3} a_{R(z)} a_{H^+Z^-} k_{-4} a_{R(g)} k_{-5} a_{H_2(g)}}. \tag{18}$$

The thermodynamic activity of any given surface intermediate appearing in the forward and reverse rate expressions in Eq. (18) is identical for a fixed set of reaction conditions (T, P_j). These terms cancel in such cases and replacing activities for ideal gases with pressures results in:

$$\frac{\vec{r}_D}{\overleftarrow{r}_H} = \frac{k_1 P_{RH_2} k_2 k_3 k_4 k_5}{k_{-1} k_{-2} k_{-3} k_{-4} P_R k_{-5} P_{H_2}}. \tag{19}$$

The isolation of dehydrogenation and hydrogenation rate parameters in the numerator and denominator, respectively, then gives:

$$\frac{\vec{r}_D}{\overleftarrow{r}_H} = \frac{K_1 k_2 P_{RH_2}}{k_{-2} K_3^{-1} K_4^{-1} K_5^{-1} P_R P_{H_2}} = \frac{k_{meas,D} P_{RH_2}}{k_{meas,H} P_R P_{H_2}}. \tag{20}$$

Thus, the ratio of measured rate constants for alkane dehydrogenation ($k_{meas,D}$) and alkene hydrogenation ($k_{meas,H}$), as given by Eq. (20), equals the equilibrium constant for the interconversion of the gaseous molecules, as given by Eq. (17), but only when the surface coverage of each species is identical in both directions. This requirement is rigorously met *only for a fixed set of reaction conditions* (T, P_j); however, the reaction rate in the direction opposing equilibrium cannot be measured directly in such cases.

Turnover rates for monomolecular propane dehydrogenation and bimolecular propene hydrogenation were measured at different pressures so as to ensure unidirectional reactions in their respective directions ($\eta_i < 0.001$). Propene hydrogenation rates depend linearly on both C_3H_6 and H_2 pressures (Fig. 3), consistent with the rate expression derived when propoxide formation (Step 3, Scheme 1) is quasi-equilibrated but inconsistent with the zero-order H_2 dependence in the expression derived when Step 2 (Scheme 1) is assumed to be quasi-equilibrated instead (derivation in Appendix A). The mean value of $k_{meas,D}/k_{meas,H}$ at 748 K for all zeolites tested is 0.017 ± 0.001 bar (Table 2), which is identical, within experimental accuracy, to the equilibrium constant (K_R) for the stoichiometric propane dehydrogenation reaction at 748 K (0.017 bar; Section S.2, Supporting information). This remarkable agreement is consistent with Eq. (17) for $\bar{\sigma} = 1$ (evident from the elementary steps in Scheme 1), as if stoichiometric dehydrogenation–hydrogenation reactions behaved as a single elementary step.

This thermodynamic consistency between alkane dehydrogenation and alkene hydrogenation rate constants and equations persists at all temperatures (718–778 K; Fig. 5), but it is not rigorously required in this case, because De Donder relations apply only when forward and reverse reactions are carried out at the same reactant and product pressures. The ratio of propane dehydrogenation and propene hydrogenation rates, when measured at different conditions (denoted by subscripts A and B, respectively) and when alkoxide desorption and formation (Step 3, Scheme 1) is quasi-equilibrated, is given by (derivation in Appendix A):

$$\frac{(\vec{r}_D)_A}{\left(\overleftarrow{r}_H\right)_B} = \frac{k_{meas,D}(P_{RH_2})_A (c_{H^+Z^-})_A}{k_{meas,H}(P_{H_2})_B (P_R)_B (c_{H^+Z^-})_B}. \tag{21}$$

This equation reduces to that describing a fixed set of reaction conditions (Eq. (20)) *only* when unoccupied H^+ sites are the most abundant species at the different reaction conditions used to measure forward and reverse rates, which is the case for the high temperatures and low hydrocarbon pressures used in this study. Thus, the persistent relevance of the De Donder relation beyond its intended scope reflects a unique situation in which different conditions for forward and reverse catalytic reactions preserve the identity of a *single* most abundant surface intermediate and of a *single* kinetically-relevant step, which must be unoccupied H^+ sites and Step 2 (Scheme 1), respectively, for the dehydrogenation–hydrogenation reactions described in this study (Appendix A). In such cases, forward and reverse directions of the kinetically-relevant step, and consequently of a multi-step chemical reaction sequence even far away from equilibrium, must obey the principle of microscopic reversibility. This unique situation, not all that infrequent in heterogeneous catalysis, allows the rigorous prediction of the rate in one direction from thermodynamic data and the rate in the opposite direction by using Eq. (17), for any active site or catalyst, irrespective of its reactivity or structure.

Measured activation barriers for monomolecular propane dehydrogenation (Eq. (3)) and for propene hydrogenation (Eq. (6)) depend on zeolite channel structure because they each reflect enthalpy differences between the same transition state (Step 2, Scheme 1) solvated by channel environments and their respective reactants in the extrazeolitic gas phase. The difference between $E_{meas,D}$ and $E_{meas,H}$ on a given site is:

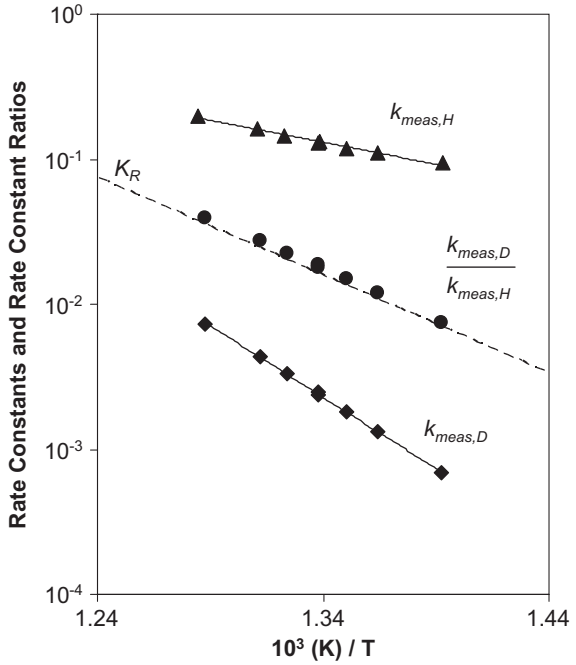

Fig. 5. Rate constants for monomolecular propane dehydrogenation ($k_{meas,D}$; mol (mol H^+) s^{-1} (bar C_3H_8)$^{-1}$; ♦) and propene hydrogenation ($k_{meas,H}$; mol (mol H^+) s^{-1} (bar C_3H_6)$^{-1}$ (bar H_2)$^{-1}$; ▲) and their ratio ($k_{meas,D}/k_{meas,H}$ bar; ●) from 718 to 778 K on $H_{100}Na_0$-MOR-T. The equilibrium constant for the gas-phase reaction (K_R; bar) is given by the dashed line.

$$E_{meas,D} - E_{meas,H} = \Delta H^{\circ}_{C_3H_6(g)} + \Delta H^{\circ}_{H_2(g)} - \Delta H^{\circ}_{C_3H_8(g)} = \Delta H^{\circ}_{R(g)}, \qquad (22)$$

in which the enthalpy of the bare proton and of the transition state cancel rigorously. The differences between measured $E_{meas,D}$ and $E_{meas,H}$ are very similar on all zeolites (127 ± 8 kJ mol^{-1}; Table 3) and identical, within experimental accuracy, to the enthalpy for the stoichiometric propane dehydrogenation reaction ($\Delta H_{R(g)}$ = 129 kJ mol^{-1}; Section S.2, Supporting information), consistent with the relation expected (Eq. (22)) when the same elementary step (Step 2, Scheme 1) is kinetically-relevant in both forward and reverse directions.

Theoretical studies indicate that monomolecular alkane dehydrogenation requires late transition states, with a nearly full positive charge localized at the alkyl cations and activation barriers that reflect predominantly electrostatic interactions of the fully-formed ion-pairs [6,7,37,38]. We conclude from the thermodynamic consistency of the rate parameters for monomolecular alkane dehydrogenation and alkene hydrogenation that they occur via a common transition state, however, the initial carbonium-ions formed in these two reactions are likely to differ in structure (as depicted qualitatively in Scheme 2). This requires, in turn, that the incipient (C–H–H)$^+$ carbonium-ions formed in forward and reverse directions of Step 2 (Scheme 1) interconvert via rotations that involve kinetically-insignificant energy barriers, which has been shown by theory for the cationic intermediates and transition states involved in hydride transfer and dehydrogenation reactions of hydrocarbons on heteropolyacids [39,40]. These data and interpretations provide the first experimental evidence for the facile rotation of cationic species at transition states, which appears to be ubiquitous in catalysis on solid acids.

The reaction coordinate for the overall catalytic reaction contains free energy barriers for the other elementary steps in Scheme 1, but they are small enough in both directions to make these steps quasi-equilibrated. As a consequence, monomolecular alkane dehydrogenation and alkene hydrogenation reactions proceed via the same kinetically-relevant transition state and differences in their measured activation energies merely reflect the enthalpy for the overall chemical reaction (Eq. (22)). This relation between activation energies in the forward and reverse direction and the reaction enthalpy (shown in Scheme 2) holds rigorously for any elementary step, but is unexpected in general for rates and barriers arising from the sequence of elementary steps required to complete a catalytic turnover. These same arguments apply for differences in measured activation entropies for the catalytic reaction in forward and reverse directions, which causes differences between $\Delta S_{meas,D}$ and $\Delta S_{meas,H}$ on all zeolites tested (134 ± 11 J mol^{-1} K^{-1}; Table 3) to equal, within experimental error, the gas-phase reaction entropy for propane dehydrogenation ($\Delta S_{R(g)}$ = 138 J mol^{-1} K^{-1}; Section S.2, Supporting information) because the transition state entropy also cancels when evaluating this difference:

$$\Delta S_{meas,D} - \Delta S_{meas,H} = \Delta S^{\circ}_{C_3H_6(g)} + \Delta S^{\circ}_{H_2(g)} - \Delta S^{\circ}_{C_3H_8(g)} = \Delta S^{\circ}_{R(g)}. \qquad (23)$$

Temperature effects on $k_{meas,D}/k_{meas,H}$ ratios depend only on the thermodynamics of the overall reaction (Eq. (22); Fig. 5); therefore, they must be identical on all catalysts, irrespective of the structure or reactivity of the active sites or of any confinement effects provided by the spatial constraints within zeolite structures, as long as H^+ remains the single MASI and Step 2 (Scheme 1) remains the sole kinetically-relevant step at the different conditions used to measure forward and reverse reaction rates. As a result, the rate of the reverse reaction at any given temperature and at any reactant and product concentrations can be determined rigorously from the rate of the forward reaction determined at that temperature but at different reactant concentrations. In the same manner, activation energies and entropies for a reaction can be estimated accurately from thermodynamic data and their values for the reaction in the opposite direction, as long as these requirements are met, as they are in this case for propane–propene interconversions.

3.5. Preferences of mechanistically-related paths for specific intrazeolite locations

Each elementary step occurring on acid sites in zeolites, and on catalytic sites in general, must proceed via a single reversible barrier and thus via identical transition states in its forward and reverse directions. As a result, an active site that preferentially catalyzes a given elementary step by stabilizing its transition state must also do so with equal preference and to the same extent in the reverse direction. This must also be true, by extension, for entire catalytic sequences even away from equilibrium at fixed reaction conditions (T, P_j) as indicated by Eq. (20), and even at different reaction conditions as long as the kinetically-relevant step remains the same and unoccupied sites are the most abundant surface species, as indicated by Eq. (21). In contrast, when surfaces are predominantly covered by species other than empty sites at the different reaction conditions used for the forward and reverse directions of a catalytic sequence, the coverage of intermediates is given by terms of different magnitude in the respective denominators of the forward and reverse rate expressions, which therefore do not cancel in the ratio of forward and reverse rates; in such cases (e.g., NH_3 synthesis and decomposition [41]), surfaces that preferentially catalyze the reaction in the forward direction do not necessarily do so in the reverse direction.

A given catalytic solid contains a range of active sites differing in structure, binding properties and spatial environment and therefore also in catalytic reactivity, even for regular crystalline materials such as zeolites. As a result, turnover rates for monomolecular alkane activation differ among protons present at different locations within a given zeolite (e.g. 8-member and 12-member rings

in H-MOR) [2,3], and the ensemble-averaged reactivity of protons in a given zeolite also varies with channel structure (e.g. H-FER, H-MFI, H-MOR) [2,42]. Thus, it seems reasonable to conclude that the aforementioned irrelevance of the catalyst identity for $k_{meas,D}/k_{meas,H}$ ratios and their exclusive thermodynamic origins can be extended to sites of different reactivity within a given catalyst. If indeed so, site properties that affect reactivity would do so with the exact proportional effects on the rates of the forward and reverse reaction, even when the rates for these reactions are measured at different conditions and each far away from its respective equilibrium, as long as such conditions preserve the identity of the single MASI (unoccupied H^+) and the single kinetically-relevant step (Step 2, Scheme 1).

Turnover rates for the monomolecular cracking and dehydrogenation of linear (C_3H_8, n-C_4H_{10}) [2] and branched (i-C_4H_{10}) [3] alkanes are significantly larger on protons located within eight-membered ring (8-MR) pockets in H-MOR than on protons with similar acid strength [43] but present within larger and more accessible 12-MR channels. The required transition states for alkane protonation at C–C and C–H bonds (Step 2, Scheme 1) are confined only partially within the shallow 8-MR pockets, leading to structures with higher entropy and lower free energy and to rate constants significantly larger on 8-MR than 12-MR protons for both dehydrogenation and cracking reactions [2]. Alkene hydrogenation proceeds via the same kinetically-relevant step and transition state as monomolecular alkane dehydrogenation; thus, hydrogenation turnover rates must also be larger, to the same exact extent, on 8-MR than on 12-MR protons in H-MOR.

Infrared spectral band deconvolution methods (Section S.3, Supporting information) showed that H-MOR samples of varying provenance or extent of Na^+ exchange contain very different distributions of protons between 8-MR side pockets (0.10–0.80 fraction; Table 1) and 12-MR channels [2]. As in the case of propane dehydrogenation, rate constants for propene hydrogenation (per total H^+; 748 K; Fig. 6) increased linearly as the fraction of the H^+ that reside within 8-MR pockets increased, consistent with the preference of both reactions for 8-MR sites. The contributions of 12-MR sites to both measured propane dehydrogenation and propene hydrogenation turnover rates were negligible (Table 4; Section S.3, Supporting information). On all MOR zeolites, irrespective of their H^+ distribution, the $k_{meas,D}/k_{meas,H}$ ratios were equal to the equilibrium constant (Table 2, Fig. 7; 748 K) and differences between the measured activation energies and entropies for the dehydrogenation and hydrogenation reactions gave the overall reaction enthalpy and entropy, respectively (Table 3). These data are consistent with Eqs. (17), (22), and (23), respectively, and with their requirement that the same elementary step (Step 2, Scheme 1) remains the sole kinetically-relevant step and that the unoccupied sites persist as the most abundant surface species at the conditions used for alkane dehydrogenation and alkene hydrogenation reactions. Therefore, Brønsted sites within a given zeolite structure that stabilize transition states more effectively and give higher turnover rates for alkane dehydrogenation (e.g., 8-MR H^+ in MOR) also do so for alkene hydrogenation, even at the very different reactant and product concentrations used to measure turnovers rates in the two reaction directions.

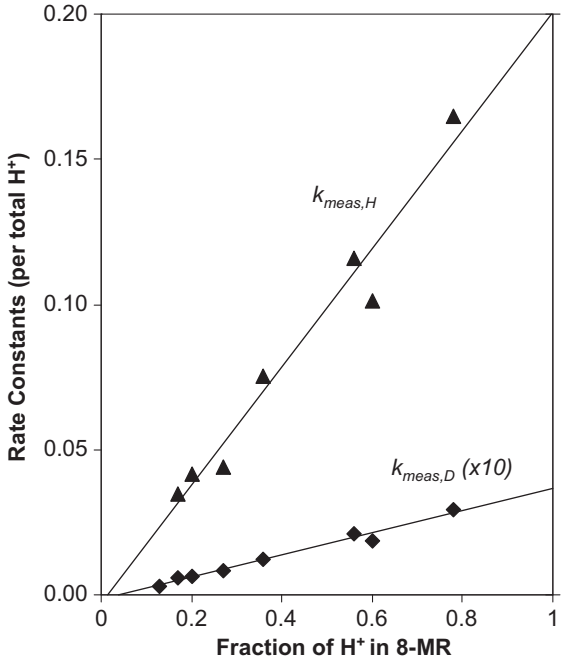

Fig. 6. Dependence of rate constants (per total H^+) for monomolecular propane dehydrogenation ($k_{meas,D}$; $\times 10$ mol (mol H^+) s^{-1} (bar C_3H_8)$^{-1}$; ♦) and propene hydrogenation ($k_{meas,H}$; mol (mol H^+) s^{-1} (bar C_3H_6)$^{-1}$ (bar H_2)$^{-1}$; ▲) on the fraction of 8-MR H^+ in MOR catalysts.

Table 4
Rate constants for monomolecular propane dehydrogenation ($k_{meas,D}$; mol (mol H^+)$^{-1}$ s^{-1} (bar C_3H_8)$^{-1}$) and for propylene hydrogenation ($k_{meas,H}$; mol (mol H^+)$^{-1}$ s^{-1} (bar C_3H_6)$^{-1}$ (bar H_2)$^{-1}$) at 748 K on 8-MR and 12-MR H^+ of MOR.

Rate constant	8-MR H^+	12-MR H^+	8-MR H^+/12-MR H^+
$k_{meas,D}$[a]	0.0036 ± 0.0004	n.d.[b]	>10[c]
$k_{meas,H}$[a]	0.20 ± 0.03	n.d.[b]	>17[c]
$k_{meas,D}/k_{meas,H}$	0.018 ± 0.004	n.d.[b]	

[a] Rate constants determined by linear regression methods (Section S.3, Supporting information).
[b] n.d., not detected.
[c] Lower bounds on 8-MR-to-12-MR rate constant ratios determined by assuming maximum values for 12-MR rate constants were upper bounds of confidence intervals containing one standard deviation, because 12-MR rate constants were undetectable, within the accuracy of regression.

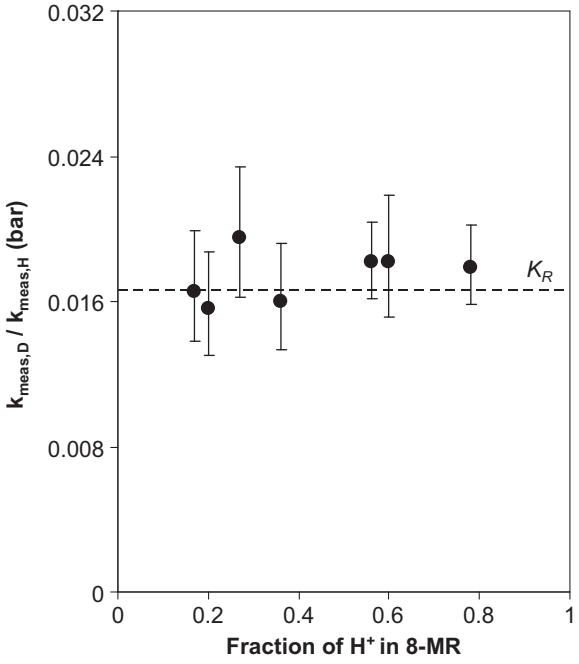

Fig. 7. Dependence of monomolecular propane dehydrogenation-to-propene hydrogenation rate constant ratios ($k_{meas,D}/k_{meas,H}$; bar; ●) at 748 K on the fraction of 8-MR H^+ in MOR catalysts. The equilibrium constant for the gas-phase reaction (K_R = 0.017 bar; 748 K) is given by the dashed line.

4. Conclusions

Brønsted acid sites within zeolite channels catalyze alkane dehydrogenation via monomolecular routes involving $(C–H–H)^+$ carbonium-ion-like transition states for kinetically-relevant C–H bond scission steps. The De Donder relations for non-equilibrium thermodynamics indicate that such sites must also catalyze the reverse reaction, alkene hydrogenation with H_2, at a fixed set of reaction conditions (T, P_j), even away from equilibrium. We show here that propene–H_2 reactions on acidic zeolites (H-FER, H-MFI, H-MOR) indeed led to the selective formation of propane, but at reactant and product concentrations that differ from those used for monomolecular alkane dehydrogenation. Moreover, the ratio of rate constants for the forward and reverse reactions was independent of catalyst identity or Brønsted acid site reactivity and depended only on the standard enthalpy and entropy of the overall reaction.

The thermodynamic origin of the ratio of rate constants measured at different conditions, possibly reflecting different mechanisms, most abundant surface intermediates or kinetically-relevant steps, is surprising and not required rigorously by non-equilibrium thermodynamic treatments of reaction rates developed by De Donder and used by Boudart. The fortuitous success of the De Donder equation in enforcing these thermodynamic constraints reflects surfaces that remain predominantly vacant and elementary steps that remain kinetically-relevant at the different conditions used to measure forward and reverse rates. In this case, propene hydrogenation proceeds via elementary steps identical (but reverse) to those required for monomolecular alkane dehydrogenation; these steps involve quasi-equilibrated adsorption of alkenes to form alkoxides and their reaction with H_2 via the same kinetically-relevant $(C–H–H)^+$ carbonium-ion-like transition states (Step 2, Scheme 1) as required for monomolecular dehydrogenation of alkanes on Brønsted acid sites. Thus, differences in catalytic reactivity among zeolitic materials, which are influenced by confinement, binding energy, and acid strength, must influence to the same proportional extent the rates of the forward and reverse reactions in general, even when the reactant and product concentrations differ in the measurement of the two rates, as long as the conditions required for the De Donder relations to hold are maintained. Within the specific context of zeolite catalysis by Brønsted acids, these concepts can be extended logically to alkylation reactions between alkanes (e.g., CH_4, C_2H_6) and alkenes (e.g., C_2H_4, C_3H_6) that proceed via $(C–C–H)^+$ carbonium-ion-like transition states [44,45] also involved in monomolecular cracking reactions of linear [2] and branched [3] alkanes.

The ability of H_2 to scavenge surface alkoxides directly via hydrogen transfer can guide design and selection strategies for zeolite catalysts that contain Brønsted acid sites, but are devoid of metal or cationic species, for hydrogenation and hydrogen transfer catalysis. These results suggest further that reactions of alkoxides with alkenes in oligomerization reactions can be terminated by hydrogen transfer from H_2, in steps analogous to those that transfer hydrogen from alkanes, and at rates that can be estimated from the reverse reaction (alkane dehydrogenation to form the alkoxide species). The incorporation of H_2 into Brønsted acid-catalyzed reaction paths indicates its presence during oligomerization, alkylation and cracking processes can influence chain growth selectivities and mitigate the formation of unreactive residues [46,47].

Acknowledgments

We acknowledge with thanks financial support from the Chevron Energy Technology Company. We also thank Prof. Matthew Neurock (University of Virginia) for helpful technical discussions.

Appendix A. Derivation of rate expressions for alkane dehydrogenation and alkene hydrogenation

A.1. Temkin relation for forward and reverse rate expressions

The reaction rates in the forward (monomolecular alkane dehydrogenation) and reverse (alkene hydrogenation) directions can be written by considering only Steps 2 and 3 in Scheme 1, which by themselves comprise a closed sequence and are preceded only by equilibrated steps that relate the activities of the species involved to those in the gas phase, using the following relation [36,48]:

$$(\vec{r}_D)_A = \frac{(\vec{r}_2)_A(\vec{r}_3)_A}{\sigma_2(\vec{r}_3)_A + \sigma_3(\overleftarrow{r}_2)_A}, \tag{A.1}$$

$$(\overleftarrow{r}_H)_B = \frac{(\overleftarrow{r}_2)_B(\overleftarrow{r}_3)_B}{\sigma_2(\vec{r}_3)_B + \sigma_3(\overleftarrow{r}_2)_B}. \tag{A.2}$$

In these equations, the subscripts A and B denote the different reaction conditions used to measure rates of dehydrogenation and hydrogenation, respectively. Reaction rates for elementary steps are given by the law of mass action, and Eqs. (A.1) and (A.2) can be rewritten as:

$$(\vec{r}_D)_A = \frac{k_2k_3(a_{RH_2(z)})_A(a_{H^+Z^-})_A}{k_3 + k_{-2}(a_{H_2(z)})_A}, \tag{A.3}$$

$$(\overleftarrow{r}_H)_B = \frac{k_{-2}k_{-3}(a_{H_2(z)})_B(a_{R(z)})_B(a_{H^+Z^-})_B}{k_3 + k_{-2}(a_{H_2(z)})_B}, \tag{A.4}$$

in which the $a_{RH^+Z^-}$ terms have been cancelled from the numerator and denominator of each equation.

The activity of H^+ species $(a_{H^+Z^-})$ can be expressed as the product of their activity coefficient $(\gamma_{H^+Z^-})$ and concentration $(c_{H^+Z^-})$:

$$a_{H^+Z^-} = \gamma_{H^+Z^-}c_{H^+Z^-}. \tag{A.5}$$

We have shown previously [2], using reported adsorption enthalpies and entropies for hydrocarbons on acidic zeolites [49–51], that H^+ sites are predominantly unoccupied at the conditions (>700 K, <0.05 bar (hydrocarbon)) relevant for monomolecular alkane dehydrogenation and alkene hydrogenation reactions. In this low coverage limit, both the fractional coverage of and activity coefficients for H^+ sites approach unity. Studies of alkane adsorption on acidic zeolites (Si/Al > 10) using calorimetry, gravimetry and infrared spectroscopy have shown further that C_3–C_6 n-alkanes adsorb specifically onto H^+ sites with constant adsorption enthalpies, even up to saturation coverages [49–51]. Thus, when framework Al atoms are isolated from each other, as tends to occur when Si/Al > 9 in FER, MFI and MOR [52], zeolites behave as Langmuirian ensembles of Brønsted acid sites with uniform binding properties, and in turn, activity coefficients that are independent of surface coverage.

A.2. Case I: Step 3 is quasi-equilibrated

The assumption of quasi-equilibrium on Step 3 results in the following relation:

$$k_3 \gg k_{-2}a_{H_2(z)}. \tag{A.6}$$

Eqs. (A.3) and (A.4) can be simplified by using the assumption in Eq. (A.6), by rewriting the activities of H^+ using Eq. (A.5), and by relating the activities of intrazeolitic species to gas-phase pressures via Steps 1, 4, and 5:

$$(\vec{r}_D)_A = K_1k_2(P_{RH_2})_A(\gamma_{H^+Z^-})_A(c_{H^+Z^-})_A, \tag{A.7}$$

$$(\overleftarrow{r}_H)_B = k_{-2}K_3^{-1}K_4^{-1}K_5^{-1}(P_R)_B(P_{H_2})_B(\gamma_{H^+Z^-})_B(c_{H^+Z^-})_B. \tag{A.8}$$

These rate expressions for monomolecular alkane dehydrogenation and alkene hydrogenation agree with their respective first-order dependences on alkane (Fig. 2) and on alkene and H_2 pressures (Fig. 3). The only rate constants that appear individually and not as a ratio (i.e., an equilibrium constant) in Eqs. (A.7) and (A.8) are for Step 2 (k_2, k_{-2}), indicating that this step, which involves the formation of $(C–H–H)^+$ carbonium-ion-like ion-pairs at the transition state, is the sole kinetically-relevant step in both directions. The ratio of forward (Eq. (A.7)) to reverse (Eq. (A.8)) rates, after cancelling $\gamma_{H^+Z^-}$ terms that are independent of coverage, gives:

$$\frac{\left(\vec{r}_D\right)_A}{\left(\overleftarrow{r}_H\right)_B} = \frac{K_1 k_2 (P_{RH_2})_A (c_{H^+Z^-})_A}{k_{-2} K_3^{-1} K_4^{-1} K_5^{-1} (P_R)_B (P_{H_2})_B (c_{H^+Z^-})_B} = K_R \frac{(P_{RH_2})_A (c_{H^+Z^-})_A}{(P_R)_B (P_{H_2})_B (c_{H^+Z^-})_B}. \quad (A.9)$$

The $c_{H^+Z^-}$ terms in Eq. (A.9) cancel only when surface sites are occupied to the same extent at conditions A and B. This is the case for the range of pressures and temperatures used in this study, which result in H^+ sites that are predominantly unoccupied by hydrocarbons, and Eq. (A.9) becomes:

$$\frac{\left(\vec{r}_D\right)_A}{\left(\overleftarrow{r}_H\right)_B} = K_R \frac{(P_{RH_2})_A}{(P_R)_B (P_{H_2})_B}. \quad (A.10)$$

This expression is equivalent to that derived from the De Donder relations (Eq. (20)), which apply for a fixed set of reaction conditions, in which case $c_{H^+Z^-}$ values are identical in forward and reverse directions and thus cancel rigorously.

A.3. Case II: Step 2 is quasi-equilibrated

The following relation holds if, instead, Step 2 is quasi-equilibrated:

$$k_{-2} a_{H_2(z)} \gg k_3. \quad (A.11)$$

In this case, the rate expressions for alkane dehydrogenation (Eq. (A.3)) and alkene hydrogenation (Eq. (A.4)) simplify to:

$$(\vec{r}_D)_A = \frac{K_2 k_3 (a_{RH_2(z)})_A (a_{H^+Z^-})_A}{(a_{H_2(z)})_A}, \quad (A.12)$$

$$(\overleftarrow{r}_H)_B = k_{-3} (a_{R(z)})_B (a_{H^+Z^-})_B. \quad (A.13)$$

Expressing $a_{H^+Z^-}$ using Eq. (A.5) and relating the activities of other species to gas-phase pressures via Steps 1, 4, and 5 gives:

$$(\vec{r}_D)_A = \frac{K_1 K_2 k_3 K_5 (P_{RH_2})_A (\gamma_{H^+Z^-})_A (c_{H^+Z^-})_A}{(P_{H_2})_A}, \quad (A.14)$$

$$(\overleftarrow{r}_H)_B = k_{-3} K_4^{-1} (P_R)_B (\gamma_{H^+Z^-})_B (c_{H^+Z^-})_B. \quad (A.15)$$

In these rate expressions, the only rate constants that appear individually are for Step 3 (k_3, k_{-3}), indicating that this step, which corresponds to alkoxide desorption and formation, must be kinetically-relevant in forward and reverse directions. Eqs. (A.14) and (A.15), however, are not supported by the experimental data and the first-order dependence of hydrogenation rates on H_2 pressure (Fig. 3).

We note, however, that the ratio of Eqs. (A.14) and (A.15), after cancelling $\gamma_{H^+Z^-}$ terms, gives an expression that resembles Eq. (A.9):

$$\frac{\left(\vec{r}_D\right)_A}{\left(\overleftarrow{r}_H\right)_B} = \frac{K_1 K_2 k_3 K_5 (P_{RH_2})_A (c_{H^+Z^-})_A}{k_{-3} K_4^{-1} (P_{H_2})_A (P_R)_B (c_{H^+Z^-})_B} = K_R \frac{(P_{RH_2})_A (c_{H^+Z^-})_A}{(P_{H_2})_A (P_R)_B (c_{H^+Z^-})_B}. \quad (A.16)$$

The consistency between Eqs. (A.16), (A.9) (derived for Step 3 quasi-equilibrated) and Eq. (20) (the De Donder relation) reflects solely the fact that the same step is kinetically-relevant in both forward and reverse directions. Eqs. (A.9) and (A.16) are equivalent to Eq. (20) only when unoccupied H^+ sites are the most abundant species for the different reaction conditions used to obtain kinetic measurements in forward and reverse directions.

Appendix B. Supplementary material

Supplementary data associated with this article can be found, in the online version, at doi:10.1016/j.jcat.2010.10.013.

References

[1] W.O. Haag, R.M. Dessau, in: Proc. 8th Int. Congr. Catalysis, Berlin, vol. 2, Verlag Chemie, Weinheim, 1984, p. 305.
[2] R. Gounder, E. Iglesia, J. Am. Chem. Soc. 131 (2009) 1958.
[3] R. Gounder, E. Iglesia, Angew. Chem. Int. Ed. 49 (2010) 808.
[4] T.F. Narbeshuber, A. Brait, K. Seshan, J.A. Lercher, J. Catal. 172 (1997) 127.
[5] B. Xu, C. Sievers, S.B. Hong, R. Prins, J.A. van Bokhoven, J. Catal. 244 (2006) 163.
[6] R.A. van Santen, G.J. Kramer, Chem. Rev. 95 (1995) 637.
[7] M.V. Frash, R.A. van Santen, Top. Catal. 9 (1999) 191.
[8] S.R. Blaszkowski, R.A. van Santen, Top. Catal. 4 (1997) 145.
[9] J.A. Lercher, R.A. van Santen, H. Vinek, Catal. Lett. 27 (1994) 91.
[10] S. Kotrel, H. Knözinger, B.C. Gates, Micropor. Mesopor. Mater. 35-36 (2000) 11.
[11] B.C. Gates, Chem. Rev. 95 (1995) 511.
[12] A. Uzun, B.C. Gates, J. Am. Chem. Soc. 131 (2009) 15887.
[13] W.A. Weber, A. Zhao, B.C. Gates, J. Catal. 182 (1999) 13.
[14] M. Choi, Z. Wu, E. Iglesia, J. Am. Chem. Soc. 132 (2010) 9129.
[15] B.-Z. Zhan, E. Iglesia, Angew. Chem. Int. Ed. 46 (2007) 3697.
[16] L.J. Simon, J.G. van Ommen, A. Jentys, J.A. Lercher, Catal. Today 73 (2002) 105.
[17] K.M. Minachev, V.I. Garanin, V.V. Kharlamov, T.A. Isakova, Kinet. Catal. 13 (1972) 1101.
[18] J. Kanai, J.A. Martens, P.A. Jacobs, J. Catal. 133 (1992) 527.
[19] C.F. Heylen, P.A. Jacobs, J.B. Uytterhoeven, J. Catal. 43 (1976) 99.
[20] P.A. Jacobs, J.B. Uytterhoeven, J. Catal. 50 (1977) 109.
[21] G.A. Olah, Y. Halpern, J. Shen, Y.K. Mo, J. Am. Chem. Soc. 93 (1971) 1251.
[22] G.A. Olah, Y. Halpern, J. Shen, Y.K. Mo, J. Am. Chem. Soc. 95 (1973) 4960.
[23] H. Hogeveen, C.J. Gaasbeek, A.F. Bickel, Recl. Trav. Chim. Pays-Bas. 88 (1969) 703.
[24] T. Sano, H. Hagiwara, K. Okabe, H. Okado, K. Saito, H. Takaya, Sekiyu Gakkaishi 29 (1986) 89.
[25] A. Corma, J. Sánchez, F. Tomás, J. Mol. Catal. 19 (1983) 9.
[26] R.C. Tolman, Phys. Rev. 23 (1924) 693.
[27] R.C. Tolman, Proc. Natl. Acad. Sci. 11 (1925) 436.
[28] H. Kranilla, W.O. Haag, B.C. Gates, J. Catal. 135 (1992) 115.
[29] J. Abbot, B.W. Wojciechowski, Can. J. Chem. Eng. 63 (1985) 462.
[30] J.S. Buchanan, J.G. Santiesteban, W.O. Haag, J. Catal. 158 (1996) 279.
[31] Th. de Donder, L'Affinité, Gauthier-Villars, Paris, 1927.
[32] Th. de Donder, P. van Rysselberghe, Thermodynamic Theory of Affinity: A Book of Principles, Stanford University Press, Stanford, 1936.
[33] K. Denbigh, The Thermodynamics of the Steady State, Methuen, London, 1951.
[34] J.A. Dumesic, J. Catal. 185 (1999) 496.
[35] W.L. Holstein, M. Boudart, J. Phys. Chem. B 101 (1997) 9991.
[36] M. Boudart, G. Djéga-Mariadassou, Kinetics of Heterogeneous Catalytic Reactions, Princeton University Press, Princeton, NJ, 1984.
[37] A.M. Rigby, G.J. Kramer, R.A. van Santen, J. Catal. 170 (1997) 1.
[38] V.B. Kazansky, M.V. Frash, R.A. van Santen, Appl. Catal. A 146 (1996) 225.
[39] M.J. Janik, R.J. Davis, M. Neurock, J. Catal. 244 (2006) 65.
[40] M.J. Janik, R.J. Davis, M. Neurock, Catal. Today 116 (2006) 90.
[41] A. Boisen, S. Dahl, J.K. Nørskov, C.H. Christensen, vol. 230, 2005, p. 309.
[42] A. Bhan, E. Iglesia, Acc. Chem. Res. 41 (2008) 559.
[43] M. Brändle, J. Sauer, J. Am. Chem. Soc. 120 (1998) 1556.
[44] G.A. Olah, J.D. Felberg, K. Lammertsma, J. Am. Chem. Soc. 105 (1983) 6529.
[45] M. Siskin, J. Am. Chem. Soc. 98 (1976) 5413.
[46] J. Meusinger, J. Liers, A. Mösch, W. Reschetilowski, J. Catal. 148 (1994) 30.
[47] J. Meusinger, A. Corma, J. Catal. 152 (1995) 189.
[48] M.I. Temkin, Adv. Catal. 28 (1979) 173.
[49] F. Eder, M. Stockenhuber, J.A. Lercher, J. Phys. Chem. B 101 (1997) 5414.
[50] F. Eder, J.A. Lercher, J. Phys. Chem. B 101 (1997) 1273.
[51] F. Eder, J.A. Lercher, Zeolites 18 (1997) 75.
[52] D. Barthomeuf, Mater. Chem. Phys. 17 (1987) 49.